PTEP

Prog. Theor. Exp. Phys. **2017**, 053D01 (20 pages)
DOI: 10.1093/ptep/ptx063

Laplace expansion method for the calculation of the reduced-width amplitudes

Yohei Chiba[1,*] and Masaaki Kimura[1,2]

[1]*Department of Physics, Hokkaido University, Sapporo 060-0810, Japan*
[2]*Nuclear Reaction Data Centre, Hokkaido University, Sapporo 060-0810, Japan*
*E-mail: chiba@nucl.sci.hokudai.ac.jp

Received March 12, 2017; Revised April 11, 2017; Accepted April 12, 2017; Published May 19, 2017

We derive the equations to calculate the reduced-width amplitudes (RWAs) of unequal-sized clusters and deformed clusters without any approximation. These equations, named the Laplace expansion method, are applicable to nuclear models that use Gaussian wave packets. The advantage of the method is demonstrated by numerical calculations of the $^{16}\mathrm{O} + \alpha$ and $^{24}\mathrm{Mg} + \alpha$ RWAs in ^{20}Ne and ^{28}Si.

Subject Index D10, D11, D29

1. Introduction

It is well known that various cluster states appear in the excited states of light stable nuclei, as illustrated in Ikeda diagram [1]. They are composed of α, ^{12}C, and ^{16}O clusters that are tightly bound and stable compared to the neighboring nuclei. In recent decades, the study of nuclear clustering has extended to unstable nuclei, where novel types of clustering have been found. The molecular-orbit and atomic-orbit states in Be isotopes [2–11] are representative of such novel types of clustering. In contrast to the clustering of light stable nuclei, they are composed of ^{6}He and ^{8}He, which are weakly bound and unstable. Since the definition of the cluster is extended from the ordinary one, we need a good measure for such non-conventional clustering.

The reduced-width amplitude (RWA) is one such clustering measure. It is the cluster formation probability at a given inter-cluster distance, and hence it is regarded as direct evidence of clustering. By the *R*-matrix theory [12], the RWA is derived from the width of the cluster states, experimentally determined by measurement of the cluster decay lifetime, the resonant scattering, and the transfer reactions. Therefore, numerous experiments have been conducted to determine the RWA and to identify various clusters. A variety of cluster states in light *p*-*sd*-shell nuclei, illustrated in the Ikeda diagram, have been identified from their large decay widths and RWAs [13–17]. Several clusters in heavier *pf* -nuclei were established in the 1990s, when measurement of the RWAs played an essential role in identifying the α cluster states of ^{40}Ca and ^{44}Ti [18–28]. More recently, the α decay property has been used in combination with the isoscalar monopole and dipole transitions to identify the gas-like α cluster states [29–35] and various clusters in *sd*-shell nuclei [36–41]. The importance of the RWA for the study of exotic clustering in neutron-rich nuclei must also be emphasized. It was an important observable in identifying the molecular clustering in Be isotopes [7–10]. More recently, the cluster states in ^{18}O and ^{22}Ne [42–53] and linear-chain states in ^{14,16}C [54–67] have been discussed from their α decays and RWAs. Thus, comparison of the measured RWA with the theoretical value is indispensable to establish cluster formation.

However, the calculation of RWA for general cluster systems in theoretical studies is not easy due to the antisymmetrization of nucleons belonging to the different clusters. To simplify the treatment of antisymmetrization, the ordinary methods for RWA calculation [68–73] often approximate the cluster wave functions with the $SU(3)$ shell model wave functions [74,75] with common oscillator parameters (the same size as the clusters). Unfortunately, this approximation limits the applicability of the methods. They are inaccurate when applied to unequal-sized clusters and clusters that cannot be approximated by a single $SU(3)$ shell model wave function. Typical examples of this may be the $^{16}\mathrm{O}+\alpha$ and $^{6}\mathrm{He}+\alpha$ clusters, i.e., the sizes of these clusters are different and a halo nucleus ^{6}He cannot be described by a single $SU(3)$ shell model wave function. Furthermore, to calculate the RWA of deformed clusters, the ordinary methods demand much computational time because of the multiple angular momentum projections. Although an approximate method proposed by Kanada-En'yo et al. [76] reduced the computational cost to some extent, the development of an alternative method for RWA calculation is highly desirable.

For this purpose, we present a new method for the RWA calculation. We derive equations that can calculate the RWA of unequal-sized clusters and deformed clusters without any approximation. These equations, named the Laplace expansion method, are applicable to nuclear models that use the Gaussian wave packets, such as antisymmetrized molecular dynamics (AMD) [77–79].

This paper is organized as follows. In the next section, we derive the equations of the Laplace expansion method. We also discuss the advantages and disadvantages of the method compared to the ordinary method. In Sect. 3, we show the numerical results for the $^{16}\mathrm{O}+\alpha$ and $^{24}\mathrm{Mg}+\alpha$ RWAs as examples of unequal-sized and deformed clusters. In the final section, we summarize the present work.

2. Laplace expansion method for RWA calculation

In this section, we outline a new method to calculate the RWA that utilizes the Laplace expansion of the matrix determinant. We first introduce the AMD wave function. Then, by using the Laplace expansion, we show that the AMD wave function of an A-body system can be decomposed into those of subsystems with masses C_1 and C_2. With this expansion, we derive the equations to calculate the RWA that we call the Laplace expansion method. We also compare the Laplace expansion method with the ordinary one to discuss its advantages and disadvantages.

2.1. Wave function of antisymmetrized molecular dynamics

The wave function of AMD for an A-body system is a Slater determinant of the Gaussian wave packets describing nucleons:

$$\Psi_A^{\mathrm{AMD}} = \frac{1}{\sqrt{A!}} \begin{vmatrix} \langle \boldsymbol{r}_1|\psi_1\rangle & \dots & \langle \boldsymbol{r}_1|\psi_A\rangle \\ \vdots & \ddots & \vdots \\ \langle \boldsymbol{r}_A|\psi_1\rangle & \dots & \langle \boldsymbol{r}_A|\psi_A\rangle \end{vmatrix}, \tag{1}$$

$$\langle \boldsymbol{r}|\psi_i\rangle = \left(\frac{|2M|}{\pi^3}\right)^{1/4} \exp\left\{-(\boldsymbol{r}-\boldsymbol{Z}_i)^{\mathrm{T}} M (\boldsymbol{r}-\boldsymbol{Z}_i)\right\} (\alpha_i\chi_\uparrow + \beta_i\chi_\downarrow)\eta_i, \tag{2}$$

where the Gaussian centroids $\boldsymbol{Z}_i$ are complex-valued three-dimensional vectors, and the spin directions are parameterized by the complex variables α_i and β_i. The isospin part η_i is fixed to either a proton or neutron. Each nucleon wave packet has these independent variables. To discuss the general

case, we assume the use of deformed Gaussian wave packets [73], and hence M denotes a symmetric positive-definite 3×3 matrix.

If the width matrix M is common for all nucleon wave packets, the AMD wave function can be straightforwardly decomposed into the internal wave function $\Psi_A^{\rm int}$ and the center-of-mass wave function $\Psi_A^{\rm cm}$:

$$\Psi_A^{\rm AMD} = \Psi_A^{\rm int}\Psi_A^{\rm cm}, \tag{3}$$

$$\Psi_A^{\rm cm} = \left(\frac{|2AM|}{\pi^3}\right)^{1/4} \exp\left\{-A(\boldsymbol{R}-\boldsymbol{Z})^{\rm T}M(\boldsymbol{R}-\boldsymbol{Z})\right\}, \tag{4}$$

$$\boldsymbol{R} = \frac{1}{A}\sum_{i=1}^{A}\boldsymbol{r}_i, \quad \boldsymbol{Z} = \frac{1}{A}\sum_{i=1}^{A}\boldsymbol{Z}_i. \tag{5}$$

This simple but important decomposition is repeatedly used in the Laplace expansion method. Without loss of generality, we assume that the $\boldsymbol{Z}_i$ satisfy the relation $\sum_{i=1}^{A}\boldsymbol{Z}_i = 0$.

The AMD wave function given by Eq. (1) is not an eigenstate of the parity and angular momentum. Therefore, the parity and angular momentum projections are usually performed:

$$\Psi_{MKA}^{J\pi} = \frac{1}{\sqrt{\mathcal{N}_K^{J\pi}}}\hat{P}_{MK}^{J}\hat{P}^{\pi}\Psi_A^{\rm int}, \tag{6}$$

$$\mathcal{N}_K^{J\pi} = \left\langle \Psi_A^{\rm int}\middle|\hat{P}_{KK}^{J}\hat{P}^{\pi}\middle|\Psi_A^{\rm int}\right\rangle, \tag{7}$$

$$\hat{P}_{MK}^{J} = \int d\Omega D_{MK}^{J*}(\Omega)\hat{R}(\Omega), \quad \hat{P}^{\pi} = \frac{1+\pi\hat{P}_r}{2}, \quad \pi = \pm, \tag{8}$$

where $\hat{P}_{MK}^{J}$ and $\hat{P}^{\pi}$ are the angular momentum and parity projectors. $D_{MK}^{J}(\Omega)$ and $\hat{R}(\Omega)$ are the Wigner D function and rotation operator dependent on the Euler angles Ω. $\hat{P}_r$ is the parity operator.

In nuclear structure studies, in addition to the projection, the parity and angular momentum projected AMD wave functions are superposed to take the effects of configuration mixing and shape fluctuation into account (generator coordinate method; GCM):

$$\Psi_{MA}^{J\pi} = \sum_{s=1}^{s_{\rm max}}\sum_{K=-J}^{J} c_{sK}\frac{1}{\sqrt{\mathcal{N}_K^{J\pi}(s)}}\hat{P}_{MK}^{J}\hat{P}^{\pi}\Psi_A^{\rm int}(s) = \sum_{s=1}^{s_{\rm max}}\sum_{K=-J}^{J} c_{sK}\Psi_{MKA}^{J\pi}(s), \tag{9}$$

$$\Psi_{MKA}^{J\pi}(s) = \frac{1}{\sqrt{\mathcal{N}_K^{J\pi}(s)}}\hat{P}_{MK}^{J}\hat{P}^{\pi}\Psi_A^{\rm int}(s), \tag{10}$$

$$\mathcal{N}_K^{J\pi}(s) = \left\langle \Psi_A^{\rm int}(s)\middle|\hat{P}_{KK}^{J}\hat{P}^{\pi}\middle|\Psi_A^{\rm int}(s)\right\rangle, \tag{11}$$

where s is the index for the internal wave functions and c_{sK} is the coefficient of the superposition. Hereafter, we term the wave functions given by Eqs. (1), (6), and (9) the "AMD wave function," "projected AMD wave function," and "GCM wave function," respectively.

It must be noted that the following discussion and the Laplace expansion method are also applicable to the Brink–Bloch wave function [80] and the $SU(3)$ shell model wave function (harmonic oscillator wave function without spin–orbit splitting), because the AMD wave function includes the Brink–Bloch wave function and $SU(3)$ shell model wave function as special cases: When the centroids of the wave packets are common for the quartet of $n\uparrow$, $n\downarrow$, $p\uparrow$, and $p\downarrow$, the AMD wave function

is equal to the Brink–Bloch wave function for $N\alpha$ systems. At the limit $\boldsymbol{Z}_i \to 0$, the AMD wave function is equal to the $SU(3)$ shell model wave function.

2.2. Laplace expansion of the AMD wave function

The Laplace expansion of the determinant of an $A \times A$ matrix B is given as

$$|B| = \sum_{1 \le i_1 < \cdots < i_{C_1} \le A} P(i_1, \ldots, i_{C_1}) |B(i_1, \ldots, i_{C_1})| |B(i_{C_1+1}, \ldots, i_A)|, \tag{12}$$

where the summation runs over all possible combinations of indices $i_1, \ldots, i_{C_1}$. The phase factor $P(i_1, \ldots, i_{C_1})$ is defined as

$$P(i_1, \ldots, i_{C_1}) = (-)^{C_1(C_1+1)/2 + \sum_{s=1}^{C_1} i_s}. \tag{13}$$

$|B(i_1, \ldots, i_{C_1})|$ is the determinant of the $C_1 \times C_1$ matrix composed from the $1, \ldots, C_1$th rows and the $i_1, \ldots, i_{C_1}$th columns of the matrix B,

$$|B(i_1, \ldots, i_{C_1})| = \begin{vmatrix} B_{1i_1} & \cdots & B_{1i_{C_1}} \\ \vdots & \ddots & \vdots \\ B_{C_1 i_1} & \cdots & B_{C_1 i_{C_1}} \end{vmatrix}, \tag{14}$$

and $|B(i_{C_1+1}, \ldots i_A)|$ is the determinant of the $C_2 \times C_2$ matrix ($C_1 + C_2 = A$) formed by removing the $1, \ldots, C_1$th rows and the $i_1, \ldots, i_{C_1}$th columns from B,

$$|B(i_{C_1+1}, \ldots, i_A)| = \begin{vmatrix} B_{C_1+1, i_{C_1+1}} & \cdots & B_{C_1+1, i_A} \\ \vdots & \ddots & \vdots \\ B_{A, i_{C_1+1}} & \cdots & B_{A, i_A} \end{vmatrix}, \tag{15}$$

where $i_{C_1+1}, \ldots, i_A$ denote the column indices other than $i_1, \ldots, i_{C_1}$ and satisfy the relation $1 \le i_{C_1+1} < \cdots < i_A \le A$.

Applying the Laplace expansion to the A-body AMD wave function given by Eq. (1), we obtain the decomposition of the AMD wave function:

$$\Psi^{\mathrm{AMD}}_A = \sqrt{\frac{C_1! C_2!}{A!}} \sum_{1 \le i_1 < \cdots < i_{C_1} \le A} P(i_1, \ldots, i_{C_1}) \Psi^{\mathrm{AMD}}_{C_1}(i_1, \ldots, i_{C_1}) \Psi^{\mathrm{AMD}}_{C_2}(i_{C_1+1}, \ldots, i_A). \tag{16}$$

Here, $\Psi^{\mathrm{AMD}}_{C_1}(i_1, \ldots, i_{C_1})$ and $\Psi^{\mathrm{AMD}}_{C_2}(i_{C_1+1}, \ldots, i_A)$ are the AMD wave functions for the subsystems with masses C_1 and C_2, which are defined as

$$\Psi^{\mathrm{AMD}}_{C_1}(i_1, \ldots, i_{C_1}) = \frac{1}{\sqrt{C_1!}} \begin{vmatrix} \langle \boldsymbol{r}_1 | \psi_{i_1} \rangle & \cdots & \langle \boldsymbol{r}_1 | \psi_{i_{C_1}} \rangle \\ \vdots & \ddots & \vdots \\ \langle \boldsymbol{r}_{C_1} | \psi_{i_1} \rangle & \cdots & \langle \boldsymbol{r}_{C_1} | \psi_{i_{C_1}} \rangle \end{vmatrix}, \tag{17}$$

$$\Psi^{\mathrm{AMD}}_{C_2}(i_{C_1+1}, , \ldots, i_A) = \frac{1}{\sqrt{C_2!}} \begin{vmatrix} \langle \boldsymbol{r}_{C_1+1} | \psi_{i_{C_1+1}} \rangle & \cdots & \langle \boldsymbol{r}_{C_1+1} | \psi_{i_A} \rangle \\ \vdots & \ddots & \vdots \\ \langle \boldsymbol{r}_A | \psi_{i_{C_1+1}} \rangle & \cdots & \langle \boldsymbol{r}_A | \psi_{i_A} \rangle \end{vmatrix}. \tag{18}$$

Since the internal and center-of-mass wave functions are analytically separable, as shown in Eq. (3), the product of the AMD wave functions on the right-hand side of Eq. (16) is equal to the product of the internal and center-of-mass wave functions of the subsystems,

$$\Psi^{\rm AMD}_{C_1}\Psi^{\rm AMD}_{C_2} = \Psi^{\rm cm}_{C_1}\Psi^{\rm cm}_{C_2}\Psi^{\rm int}_{C_1}\Psi^{\rm int}_{C_2}, \tag{19}$$

$$\Psi^{\rm cm}_{C_1} = \left(\frac{|2C_1M|}{\pi^3}\right)^{1/4} \exp\left\{-C_1(\boldsymbol{R}_{C_1}-\boldsymbol{Z}_{C_1})^{\rm T}M(\boldsymbol{R}_{C_1}-\boldsymbol{Z}_{C_1})\right\}, \tag{20}$$

$$\Psi^{\rm cm}_{C_2} = \left(\frac{|2C_2M|}{\pi^3}\right)^{1/4} \exp\left\{-C_2(\boldsymbol{R}_{C_2}-\boldsymbol{Z}_{C_2})^{\rm T}M(\boldsymbol{R}_{C_2}-\boldsymbol{Z}_{C_2})\right\}, \tag{21}$$

$$\boldsymbol{R}_{C_1} = \frac{1}{C_1}\sum_{i=1}^{C_1}\boldsymbol{r}_i, \quad \boldsymbol{R}_{C_2} = \frac{1}{C_2}\sum_{i=C_1+1}^{A}\boldsymbol{r}_i, \tag{22}$$

$$\boldsymbol{Z}_{C_1} = \frac{1}{C_1}\sum_{i\in\{i_1,\ldots,i_{C_1}\}}\boldsymbol{Z}_i, \quad \boldsymbol{Z}_{C_2} = \frac{1}{C_2}\sum_{i\in\{i_{C_1+1},\ldots,i_A\}}\boldsymbol{Z}_i, \tag{23}$$

where we suppressed the indices $i_1,\ldots,i_A$ for simplicity. $\boldsymbol{R}_{C_1}$ and $\boldsymbol{R}_{C_2}$ denote the center-of-mass coordinates of the subsystems. Then, we rewrite the product of the center-of-mass wave functions of clusters to the product of the center-of-mass wave function of the A-body system $\Psi^{\rm cm}_A$ and the relative wave function between the subsystems $\chi(\boldsymbol{r})$:

$$\Psi^{\rm cm}_{C_1}\Psi^{\rm cm}_{C_2} = \Psi^{\rm cm}_A\chi(\boldsymbol{r}), \tag{24}$$

$$\chi(\boldsymbol{r}) = \left(\frac{|2\Gamma|}{\pi^3}\right)^{1/4} \exp\left\{-(\boldsymbol{r}-\boldsymbol{z})^{\rm T}\Gamma(\boldsymbol{r}-\boldsymbol{z})\right\}, \tag{25}$$

$$\boldsymbol{r} = \boldsymbol{R}_{C_1}-\boldsymbol{R}_{C_2}, \quad \boldsymbol{z} = \boldsymbol{Z}_{C_1}-\boldsymbol{Z}_{C_2}, \quad \Gamma = \frac{C_1C_2}{A}M. \tag{26}$$

As a result, the product of the AMD wave functions is transformed as follows:

$$\Psi^{\rm AMD}_{C_1}(i_1,\ldots,i_{C_1})\Psi^{\rm AMD}_{C_2}(i_{C_1+1},\ldots,i_A) = \Psi^{\rm cm}_A\chi(\boldsymbol{r};i_1,\ldots,i_A)\Psi^{\rm int}_{C_1}(i_1,\ldots,i_{C_1})\Psi^{\rm int}_{C_2}(i_{C_1+1},\ldots,i_A). \tag{27}$$

Note that $\Psi^{\rm cm}_A$ is independent of the choice of $i_1,\ldots,i_{C_1}$. Substituting Eq. (27) into Eq. (16), and removing the center-of-mass wave function, we obtain a decomposition of the A-body internal wave function into two subsystems with masses C_1 and C_2:

$$\Psi^{\rm int}_A = \sqrt{\frac{C_1!C_2!}{A!}}\sum_{1\le i_1<\cdots<i_{C_1}\le A} P(i_1,\ldots,i_{C_1})\chi(\boldsymbol{r};i_1,\ldots i_A)\Psi^{\rm int}_{C_1}(i_1,\ldots,i_{C_1})\Psi^{\rm int}_{C_2}(i_{C_1+1},\ldots,i_A). \tag{28}$$

It is noted that the Laplace expansion can be applied recursively, and hence the decomposition of an A-body wave function into three and more subsystems is also straightforward.

2.3. Calculation of the RWA using Laplace expansion

Using Laplace expansion of the AMD wave function, we can calculate the RWA of the $C_1 + C_2$ cluster system without any approximation. First, we discuss the RWA of a single projected AMD wave function; extension to the GCM wave function is discussed later.

The RWA for a two-body cluster system is defined as the overlap amplitude between the A-body wave function $\Psi^{J\pi}_{MA}$ and the reference state composed of the clusters with masses C_1 and C_2,

$$y^{J\pi}_{j_1\pi_1 j_2\pi_2 j_{12} l}(a) = \sqrt{\frac{A!}{(1+\delta_{C_1C_2})C_1!C_2!}} \left\langle \frac{\delta(r-a)}{r^2} \left[Y_l(\hat{r}) \left[\Phi^{j_1\pi_1}_{C_1} \Phi^{j_2\pi_2}_{C_2} \right]_{j_{12}} \right]_{JM} \middle| \Psi^{J\pi}_{MA} \right\rangle, \tag{29}$$

where $\Phi^{j_1\pi_1}_{C_1}$ and $\Phi^{j_2\pi_2}_{C_2}$ are the wave functions of clusters C_1 and C_2. Their spins j_1 and j_2 are coupled to j_{12}, and j_{12} is coupled to the orbital angular momentum l of the inter-cluster motion to yield the total spin-parity J^π. Therefore, π_1, π_2, and l must satisfy the relation $\pi = \pi_1\pi_2(-)^l$. We assume that the wave functions $\Psi^{J\pi}_{MA}$, $\Phi^{j_1\pi_1}_{C_1}$, and $\Phi^{j_2\pi_2}_{C_2}$ are antisymmetrized and normalized.

With this definition, by substituting Eq. (6) into Eq. (29), the RWA of a projected AMD wave function reads

$$\begin{aligned}
y^{J\pi}_{j_1\pi_1 j_2\pi_2 j_{12} l}(a) &= \sqrt{\frac{A!}{(1+\delta_{C_1C_2})C_1!C_2!}} \left\langle \frac{\delta(r-a)}{r^2} \left[Y_l(\hat{r}) \left[\Phi^{j_1\pi_1}_{C_1} \Phi^{j_2\pi_2}_{C_2} \right]_{j_{12}} \right]_{JM} \middle| \Psi^{J\pi}_{MKA} \right\rangle \\
&= \frac{1}{\sqrt{\mathcal{N}^{J\pi}_K}} \sqrt{\frac{A!}{(1+\delta_{C_1C_2})C_1!C_2!}} \left\langle \frac{\delta(r-a)}{r^2} \hat{P}^J_{KM} \left[Y_l(\hat{r}) \left[\Phi^{j_1\pi_1}_{C_1} \Phi^{j_2\pi_2}_{C_2} \right]_{j_{12}} \right]_{JM} \middle| \Psi^{\rm int}_A \right\rangle \\
&= \frac{1}{\sqrt{\mathcal{N}^{J\pi}_K}} \sqrt{\frac{A!}{(1+\delta_{C_1C_2})C_1!C_2!}} \left\langle \frac{\delta(r-a)}{r^2} \left[Y_l(\hat{r}) \left[\Phi^{j_1\pi_1}_{C_1} \Phi^{j_2\pi_2}_{C_2} \right]_{j_{12}} \right]_{JK} \middle| \Psi^{\rm int}_A \right\rangle \\
&= \frac{1}{\sqrt{\mathcal{N}^{J\pi}_K}} \sqrt{\frac{A!}{(1+\delta_{C_1C_2})C_1!C_2!}} \sum_{m_{12}m_l m_1 m_2} C^{JK}_{lm_l j_{12} m_{12}} C^{j_{12}m_{12}}_{j_1 m_1 j_2 m_2} \\
&\quad \times \left\langle \frac{\delta(r-a)}{r^2} Y_{lm_l}(\hat{r}) \Phi^{j_1\pi_1}_{m_1 C_1} \Phi^{j_2\pi_2}_{m_2 C_2} \middle| \Psi^{\rm int}_A \right\rangle,
\end{aligned} \tag{30}$$

where we used the relation $\pi = \pi_1\pi_2(-)^l$ and the properties of the angular momentum projector $(\hat{P}^J_{MK})^\dagger = \hat{P}^J_{KM}$ and $\hat{P}^{J\pi}_{KM}\,|JM\rangle = |JK\rangle$. $C^{JM}_{j_1 m_1 j_2 m_2}$ denotes the Clebsch–Gordan coefficient. By using the Laplace expansion of $\Psi^{\rm int}_A$ given by Eq. (28), the braket on the right-hand side of Eq. (30) is written as

$$\begin{aligned}
&\left\langle \frac{\delta(r-a)}{r^2} Y_{lm_l}(\hat{r}) \Phi^{j_1\pi_1}_{m_1 C_1} \Phi^{j_2\pi_2}_{m_2 C_2} \middle| \Psi^{\rm int}_A \right\rangle = \sqrt{\frac{C_1!C_2!}{A!}} \sum_{1\le i_1<\cdots<i_{C_1}\le A} P(i_1,\ldots,i_{C_1}) \\
&\quad \times \left\langle \frac{\delta(r-a)}{r^2} Y_{lm_l}(\hat{r}) \Phi^{j_1\pi_1}_{m_1 C_1} \Phi^{j_2\pi_2}_{m_2 C_2} \middle| \chi(\boldsymbol{r}; i_1,\ldots,i_A) \Psi^{\rm int}_{C_1}(i_1,\ldots,i_{C_1}) \Psi^{\rm int}_{C_2}(i_{C_1+1},\ldots,i_A) \right\rangle.
\end{aligned} \tag{31}$$

Note that the braket in the last line has no antisymmetrizer with respect to the nucleons belonging to different subsystems. Therefore, it is equal to the product of the overlaps between the relative wave functions and between the subsystems:

$$\begin{aligned}
&\left\langle \frac{\delta(r-a)}{r^2} Y_{lm_l}(\hat{r}) \Phi^{j_1\pi_1}_{m_1 C_1} \Phi^{j_2\pi_2}_{m_2 C_2} \middle| \chi(\boldsymbol{r}; i_1,\ldots,i_A) \Psi^{\rm int}_{C_1}(i_1,\ldots,i_{C_1}) \Psi^{\rm int}_{C_2}(i_{C_1+1},\ldots,i_A) \right\rangle \\
&= \left\langle \frac{\delta(r-a)}{r^2} Y_{lm_l}(\hat{r}) \middle| \chi(\boldsymbol{r}; i_1,\ldots,i_A) \right\rangle \langle \Phi^{j_1\pi_1}_{m_1 C_1} | \Psi^{\rm int}_{C_1}(i_1,\ldots,i_{C_1}) \rangle \, \langle \Phi^{j_2\pi_2}_{m_2 C_2} | \Psi^{\rm int}_{C_2}(i_{C_1+1},\ldots,i_A) \rangle \,.
\end{aligned} \tag{32}$$

Substituting Eqs. (31) and (32) into Eq. (30), we obtain the RWA of a projected AMD wave function:

$$y^{J\pi}_{j_1\pi_1 j_2\pi_2 j_{12} l}(a) = \frac{1}{\sqrt{\mathcal{N}^{J\pi}_K (1+\delta_{C_1C_2})}} \sum_{1\le i_1<\cdots<i_A\le A} P(i_1,\ldots,i_{C_1}) \times \left[\chi_l(a;i_1,\ldots,i_A)\left[N^{j_1\pi_1}(i_1,\ldots,i_{C_1})N^{j_2\pi_2}(i_{C_1+1},\ldots i_A)\right]_{j_{12}}\right]_{JK}, \tag{33}$$

with the definitions of the overlaps:

$$\chi_{lm_l}(a;i_1,\ldots,i_A) = \left\langle \frac{\delta(r-a)}{r^2} Y_{lm_l}(\hat{r}) \middle| \chi(\boldsymbol{r};i_1,\ldots,i_A)\right\rangle, \tag{34}$$

$$N^{j_1\pi_1}_{m_1}(i_1,\ldots,i_{C_1}) = \langle \Phi^{j_1\pi_1}_{m_1C_1} | \Psi^{\rm int}_{C_1}(i_1,\ldots,i_{C_1})\rangle, \tag{35}$$

$$N^{j_2\pi_2}_{m_2}(i_{C1+1},\ldots,i_A) = \langle \Phi^{j_2\pi_2}_{m_2C_2} | \Psi^{\rm int}_{C_2}(i_{C_1+1},\ldots,i_A)\rangle. \tag{36}$$

Thus, the RWA is obtained by calculating the overlaps defined by Eqs. (34), (35), and (36), which are easily calculated as explained in Appendix A.

The extension of the method to the GCM wave function is straightforward. Substituting Eq. (9) into Eq. (29), one easily obtains the RWA of the GCM wave function as follows:

$$y^{J\pi}_{j_1\pi_1 j_2\pi_2 j_{12} l}(a) = \sum_{s=1}^{s_{\rm max}} \sum_{K=-J}^{J} c_{sK} y^{J\pi}_{j_1\pi_1 j_2\pi_2 j_{12} l}(a;sK), \tag{37}$$

$$y^{J\pi}_{j_1\pi_1 j_2\pi_2 j_{12} l}(a;sK) = \sqrt{\frac{A!}{C_1!C_2!}} \left\langle \frac{\delta(r-a)}{r^2}\left[Y_l(\hat{r})\left[\Phi^{j_1\pi_1}_{C_1}\Phi^{j_2\pi_2}_{C_2}\right]_{j_{12}}\right]_{JM} \middle| \Psi^{J\pi}_{MKA}(s)\right\rangle. \tag{38}$$

Thus, the RWA of the GCM wave function is the superposition of the RWAs of the projected AMD wave functions defined by Eq. (38), which are calculated by using Eq. (33) for every $\Psi^{J\pi}_{MKA}(s)$. In the same way, when the reference wave function $\Phi^{j_1\pi_1}_{m_1C_1}$ is a GCM wave function, the overlap $N^{j_1\pi_1}_{m_1}(i_1,\ldots,i_{C_1})$ is a sum of the overlaps of the projected AMD wave functions.

2.4. *Advantages of the Laplace expansion method*

It may be worthwhile comparing the Laplace expansion method with an ordinary method [70–73] that is often used in cluster models and AMD to see its advantages and disadvantages. The ordinary method uses a set of projected Brink–Bloch-type wave functions defined as

$$\Phi^{J\pi}_{j_1\pi_1 j_2\pi_2 j_{12} l}(S_p) = \frac{2l+1}{2J+1} \sum_{m_{12}m_1m_2} C^{Jm_{12}}_{l0j_{12}m_{12}} \hat{P}^J_{Mm_{12}} C^{j_{12}m_{12}}_{j_1m_1j_2m_2} \Phi^{\rm BB}_{j_1\pi_1 m_1 j_2\pi_2 m_2}(S_p), \tag{39}$$

$$\Phi^{\rm BB}_{j_1\pi_1 m_1 j_2\pi_2 m_2}(S_p) = \sqrt{\frac{C_1!C_2!}{A!}}\mathcal{A}\left\{\hat{P}^{j_1}_{m_1k_1}\hat{P}^{\pi_1}\Phi_{C_1}\left(-\frac{C_2}{A}\boldsymbol{S}_p\right)\hat{P}^{j_2}_{m_2k_2}\hat{P}^{\pi_2}\Phi_{C_2}\left(\frac{C_1}{A}\boldsymbol{S}_p\right)\right\}, \tag{40}$$

$$\boldsymbol{S}_p = (0,0,S_p). \tag{41}$$

$\Phi_{C_1}\left(-C_2/A\boldsymbol{S}_p\right)$ and $\Phi_{C_2}\left(C_1/A\boldsymbol{S}_p\right)$ are the wave functions for clusters with masses C_1 and C_2 with their center-of-mass wave functions, and placed with the inter-cluster distance S_p. The inter-cluster distance S_p is discretized, for example, as

$$S_p = p\Delta S, \quad p = 1,\ldots,p_{\rm max}. \tag{42}$$

The following three conditions are often required to reduce the computational cost:

- Φ_{C_1} and Φ_{C_2} are the $SU(3)$ shell model wave functions without particle–hole excitations.
- The oscillator parameters of Φ_{C_1} and Φ_{C_2} are the same value, $\hbar\omega = 2\hbar^2\nu/m$.
- Φ_{C_1} and Φ_{C_2} are the eigenstates of the principal quantum number $\hat{N}$.

With these conditions satisfied, the RWA is given as follows:

$$y^{J\pi}_{j_1\pi_1 j_2\pi_2 j_{12} l}(a) = \frac{1}{\sqrt{1+\delta_{C_1C_2}}} \sum_N \mu_{Nl} e_N R_{Nl}(a), \tag{43}$$

$$\mu_{Nl} = \left\langle R_{Nl}(r) \left[Y_l(\hat{r}) \left[\Phi^{j_1\pi_1}_{C_1} \Phi^{j_2\pi_2}_{C_2} \right]_{j_{12}} \right]_J \middle| \mathcal{A} \left\{ R_{Nl}(r) \left[Y_l(\hat{r}) \left[\Phi^{j_1\pi_1}_{C_1} \Phi^{j_2\pi_2}_{C_2} \right]_{j_{12}} \right]_J \right\} \right\rangle, \tag{44}$$

$$e_{Nl} = (-)^{(N-l)/2} \sqrt{\frac{(2l+1)}{(N-l)!!(N+l+1)!!}} \sum_{pq} \frac{(\nu S_p^2)^{N/2}}{\sqrt{N!}} e^{-\nu S_p^2/2} B^{-1}_{pq} \langle \Phi^{J\pi}_{j_1\pi_1 j_2\pi_2 j_{12} l}(S_q) | \Psi^{J\pi}_{MA} \rangle , \tag{45}$$

$$B_{pq} = \langle \Phi^{J\pi}_{j_1\pi_1 j_2\pi_2 j_{12} l}(S_p) | \Phi^{J\pi}_{j_1\pi_1 j_2\pi_2 j_{12} l}(S_q) \rangle . \tag{46}$$

Here, $R_{Nl}(a)$ is the radial wave function of harmonic oscillator (HO). The derivation of these equations is explained in Appendix B and Refs. [70–73]. From these equations, we can see several advantages of the Laplace expansion method:

- The sizes of the Gaussian wave packets describing clusters C_1 and C_2 in the reference state can be different in the Laplace expansion method. This is an advantage when we calculate the RWA of unequal-sized clusters such as $^{16}\mathrm{O} + \alpha$ and $^{40}\mathrm{Ca} + \alpha$ [81].
  On the other hand, in the ordinary method, they must be equal to analytically separate center-of-mass and relative wave functions, as explained in Appendix B.
- Deformed Gaussian wave packets can be used to describe the clusters C_1 and C_2 in the reference state. Therefore, the Laplace expansion method can easily calculate the RWA of deformed clusters such as $^{10}\mathrm{Be} + \alpha$ and $^{24}\mathrm{Mg} + \alpha$ without any approximation.
  On the other hand, for the analytical separation of the center-of-mass and relative wave functions, the ordinary method uses a spherical Gaussian. For example, in Refs. [64,67], the ^{10}Be wave function was approximated by a spherical Gaussian to estimate the $^{10}\mathrm{Be} + \alpha$ RWA.
- The angular momentum projection of the cluster wave functions can be done with much reduced computational cost. This is another advantage when we calculate the RWA of deformed clusters. When the intrinsic wave functions of clusters Φ_{C_1} and Φ_{C_2} are not the eigenstate of the angular momentum, we need to perform the angular momentum projection of each cluster. In the ordinary method, we need to calculate Eqs. (45) and (46), which contain three and five angular momentum projectors and demand huge computational cost. Therefore, the approximation is often applied [64,67]. However, in the case of the Laplace expansion method, we only need to calculate Eqs. (35) and (36), which contain only one angular momentum projector.
- The GCM wave function can be used as the cluster wave functions. Therefore, the Laplace expansion method can treat various clusters which cannot be described by a single AMD wave function. A typical example is the ^{6}He cluster, which has a neutron halo. In the ordinary method, the ^{6}He cluster is often approximated by the $(0s)^4(0p_{3/2})^2$ configuration of the HO wave function [67,72].

- The Laplace expansion method does not use the eigenvalue of the norm kernel defined by Eq. (44), which represents the antisymmetrization effect between clusters. In general, the calculation of this quantity is not easy when the clusters are not described by the $SU(3)$ shell model wave functions. Therefore, several approximations have been suggested and applied [72,76]. The Laplace expansion method is free from such approximations.

The disadvantage of the Laplace expansion method should also be mentioned. It is clear from Eq. (33) that the computational cost greatly increases when the mass of the system A is large and the masses of clusters are equal ($C_1 = C_2$), because the number of possible combinations of $i_1, \ldots, i_A$ becomes huge. A typical example is the ^{16}O+^{16}O cluster in ^{32}S. In this case, there are $(16!/(8!8!))^2 \simeq 1.6\times10^8$ combinations of $i_1, \ldots, i_A$. On the other hand, since ^{16}O is a spherical and $SU(3)$ scalar cluster, the ordinary method can be straightforwardly applied and quickly calculated [82].

3. Numerical examples

In this section, we present the numerical results for the RWAs of the $^{16}\mathrm{O}+\alpha$ and $^{24}\mathrm{Mg}+\alpha$ clustering in ^{20}Ne and ^{28}Si, which are composed of unequal-sized and deformed clusters. The wave functions of ^{20}Ne and ^{28}Si are calculated by antisymmetrized molecular dynamics and are the same as obtained in our previous studies [41,73,83,84]. The Hamiltonian is common to both nuclei and is given as

$$\hat{H} = \sum_{i=1}^{A} \hat{t}_i - \hat{t}_{\mathrm{cm}} + \sum_{i<j}^{A} \hat{v}_{\mathrm{NN}} + \sum_{i<j}^{A} \hat{v}_{\mathrm{Coul}}, \tag{47}$$

where $\hat{t}_i$ and $\hat{t}_{\mathrm{cm}}$ denote the nucleon and the center-of-mass kinetic energies. $\hat{v}_{\mathrm{NN}}$ and $\hat{v}_{\mathrm{Coul}}$ denote the Gogny D1S effective nucleon–nucleon interaction [85] and the Coulomb interaction, respectively. The detailed setup of the calculations is explained below.

3.1. *RWA of the* $^{16}\mathrm{O}+\alpha$ *clustering in* ^{20}Ne

The $^{16}\mathrm{O}+\alpha$ clustering of ^{20}Ne is very famous and well-identified experimentally [16]. There are three rotational bands with a $^{16}\mathrm{O}+\alpha$ cluster structure, which are built on the 0^+_1, 1^-_1 (5.8 MeV), and 0^+_4 (8.7 MeV) states, respectively. Here we discuss the RWAs of the 0^+_1, 1^-_1, and 0^+_4 states as an example of unequal-sized clusters.

The AMD wave functions of ^{20}Ne for GCM calculation are prepared by energy variation with a constraint on the nuclear quadrupole deformation parameter β. The value of parameter β is constrained from 0.0 to 0.85 with an interval of 0.05. In addition to this, we also included Brink–Bloch-type wave functions with the inter-cluster distance S_p ranging from 1.0 fm to 8.0 fm with an interval of 1.0 fm. Here, the ^{16}O cluster is described by a single AMD wave function obtained by the energy variation, while α cluster is assumed to have a $(0s)^4$ configuration. To analytically remove the center-of-mass motion from the GCM wave function, both clusters are assumed to have the same spherical oscillator parameter $\nu = 0.16\,\mathrm{fm}^{-2}$. In short, we superposed 18 AMD wave functions and 8 Brink–Bloch-type wave functions together, and solved the GCM. The level scheme obtained is shown in Fig. 1, together with the observed levels. Detailed discussions of these states are found in the Refs. [41,73].

We prepared two different sets of cluster wave functions as the reference states [$\Phi^{j_1\pi_1}_{m_1C_1}$ and $\Phi^{j_2\pi_2}_{m_2C_2}$ in Eqs. (35) and (36)] to evaluate the RWA. In the first set, the ^{16}O and α clusters have the common oscillator lengths $\nu_{\mathrm{O}} = \nu_\alpha = 0.16\,\mathrm{fm}^{-2}$. In other words, they are the same as the above-mentioned Brink–Bloch-type wave functions. In the second set, the oscillator lengths are different. For the

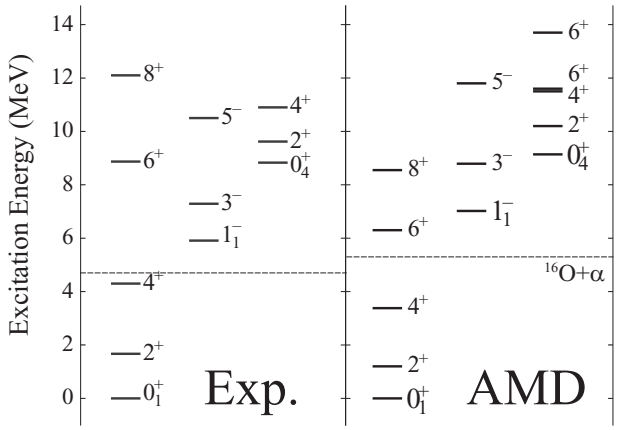

Fig. 1. The calculated and observed partial level scheme of ^{20}Ne corresponding to the $^{16}\mathrm{O} + \alpha$ cluster states. The dashed horizontal lines indicate experimental and theoretical $^{16}\mathrm{O} + \alpha$ cluster threshold energies.

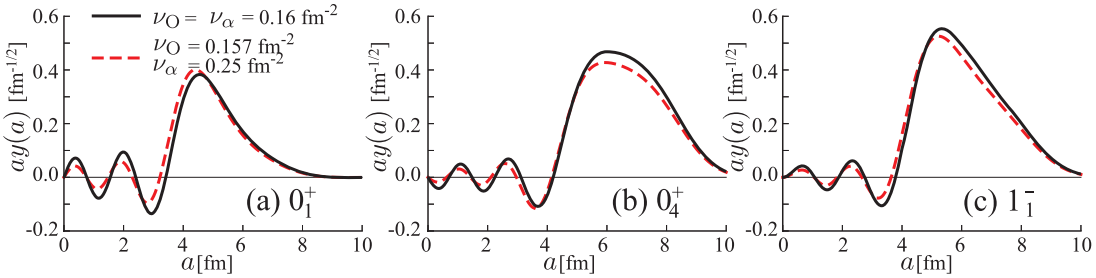

Fig. 2. The $^{16}\mathrm{O} + \alpha$ cluster RWAs of (a) the 0_1^+ state, (b) the 0_4^+ state, and (c) the 1_1^- state. The solid lines show the RWAs obtained by using the reference states with common oscillator lengths $\nu_\mathrm{O} = \nu_\alpha = 0.16\,\mathrm{fm}^{-2}$, while the dashed lines show those obtained by using the different oscillator parameters $\nu_\mathrm{O} = 0.157\,\mathrm{fm}^{-2}$ and $\nu_\alpha = 0.25\,\mathrm{fm}^{-2}$.

α cluster, we used $\nu_\alpha = 0.25\,\mathrm{fm}^{-2}$, while we used $\nu_\mathrm{O} = 0.157\,\mathrm{fm}^{-2}$ for the ^{16}O cluster, which minimizes the intrinsic energy of ^{16}O. In the following, we term the calculations with the first and second sets of cluster wave functions "common-size calculation" and "unequal-size calculation," respectively. In both cases, the RWAs were calculated by the Laplace expansion method. The calculated RWAs for the 0_1^+, 0_2^+, and 1_1^- states are shown in Fig. 2, and the α spectroscopic factor S_α and dimensionless decay width θ^2 are listed in Table 1; these are defined as follows:

$$S_\alpha = \int_0^\infty da \left| a y^{J\pi}_{j_1\pi_1 j_2\pi_2 j_{12} l}(a) \right|^2, \tag{48}$$

$$\theta_\alpha^2 = \frac{a}{3} \left| a y^{J\pi}_{j_1\pi_1 j_2\pi_2 j_{12} l}(a) \right|^2. \tag{49}$$

From larger amplitudes of the RWAs S_α and θ_α, it is evident that the 0_4^+ and 1_1^- states have more developed cluster structures than the ground state. When we compare the RWAs obtained by the common-size and unequal-size calculations, we find the following differences, although they show similar behavior:

- The nodal points of the RWA moves inward in the unequal-size calculation.
- The amplitudes of RWAs tend to be smaller in the unequal-size calculation.

Table 1. The α spectroscopic factor S_α and the dimensionless decay width θ_α^2 calculated at the channel radii $a = 6$ and 7 fm.

	$\nu_O = \nu_\alpha = 0.16\,\text{fm}^{-2}$			$\nu_O = 0.157\,\text{fm}^{-2}$, $\nu_\alpha = 0.25\,\text{fm}^{-2}$		
	S_α	θ_α^2 ($a = 6$ fm)	θ_α^2 ($a = 7$ fm)	S_α	θ_α^2 ($a = 6$ fm)	θ_α^2 ($a = 7$ fm)
0_1^+	0.24	0.06	0.01	0.26	0.05	0.01
0_4^+	0.62	0.44	0.43	0.53	0.37	0.35
1_1^-	0.71	0.49	0.28	0.63	0.41	0.22

The first point is due to the weaker antisymmetrization effect. The unequal-size calculation uses a much smaller size of the α cluster than the common-size calculation. Therefore, the α cluster is much less affected by the antisymmetrization effect. Since the oscillation of the RWAs in the internal region originates in the antisymmetrization effect, the nodal positions of the RWAs should move inward in the unequal calculation.

For the second point, there may be two explanations. In the inner region, the α clusters should be strongly distorted due to the strong effect of antisymmetrization and the mean-field potential. In such cases, the size of the α cluster should differ from that of a free α particle and may be enlarged to gain the attraction from the mean-field potential. Therefore, the common-size clusters may be favored in the inner region. In the outer region, the difference originates in the defect of the present GCM calculation. To analytically remove the center-of-mass wave function, the wave packet size of the AMD wave function is common to all nucleons. As a result, even at a large inter-cluster distance, the oscillator parameters for ^{16}O and α clusters are common in the GCM wave function, while they should be unequal to describe the correct asymptotics. It is evident that the common oscillator parameters of the GCM wave function reduces the RWA in the outer region in the unequal-size calculation. From these differences, compared to the common-size calculation, the unequal size calculation tends to yield smaller values of S_α and θ_α by approximately 10% to 20%, except for the ground state.

Related to the inaccurate asymptotics of the GCM wave functions, we comment on how to choose the channel radius a to evaluate the decay widths. In general, if the GCM wave function has the correct asymptotics, any choice of the channel radius should give the correct decay widths for the narrow resonances to which the R-matrix theory can be safely applied. However, because the bound-state approximation is often applied as mentioned above, the GCM wave function has inaccurate asymptotics, which causes the channel radius dependence and uncertainty of the evaluated widths. For example, in the present calculation, one can observe this uncertainty as the strong dependence of the dimensionless decay widths $\theta_\alpha^2(a)$ on the channel radius a. To ease this problem, several prescriptions have been suggested. For example, in Ref. [86], two different methods are discussed: the separation energy method (SEM) [87] and the Green's function method (GFM) [88,89]. In the SEM, which is often used because of its simplicity, the channel radius a is chosen so that the calculated RWA and the Coulomb wave function are smoothly connected at a channel radius outside the final peak of the calculated RWA. The GFM connects the calculated RWA to the correct asymptotics using the Green's function with auxiliary potential. Hence, it is more a sophisticated method and applied for more accurate width estimation of broader resoannces. In the present calculation, when we apply SEM, the channel radius $a = 6$ fm is preferable for the 1_1^- state, while the choice of $a = 7$ fm is better for the 0_4^+ state, although the use of the R-matrix for the 0_4^+ state with a very broad width can be dangerous.

3.2. *RWA of the* ^{24}Mg + α *clustering in* ^{28}Si

A variety of cluster states, such as ^{24}Mg + α, ^{20}Ne + 2α, and ^{16}O + ^{12}C clustering, are expected to exist in ^{28}Si. Many of them are related to the nuclear reactions in astrophysical processes, and hence have been intensively studied for many years [83,84,90–100], although their properties are not fully understood yet.

In our recent study [84], we performed the AMD calculation to identify these cluster states. We performed energy variation with constraints on the quadrupole deformation parameters β and γ [101] to generate the AMD wave functions for the GCM calculation. In addition to this, we also performed energy variation with a constraint on the inter-cluster distance [102] to generate various cluster configurations. These two kinds of basis wave functions are superposed and the GCM calculation was performed. As a result, we suggested various cluster bands: two groups of ^{24}Mg + α bands, and the ^{20}Ne + 2α and ^{16}O + ^{12}C bands. From these, we discuss here the RWAs of a group of ^{24}Mg + α bands named the "^{24}Mg + α (T) bands" as examples of deformed clusters.

Figure 3(a) shows the ^{24}Mg + α (T) bands. Three rotational bands with pronounced ^{24}Mg + α clustering are built on the 1^-_1 and 0^+_6 states, and on a group of 1^- states (1^-_8, 1^-_9, and 1^-_{10}). Note that the ^{24}Mg + α configuration is strongly mixed with other cluster configurations such as ^{16}O + ^{12}C. As a result, it does not appear as a single state in the band built on the $1^-_{8,9,10}$ states. Therefore, in Fig. 3(a) we show the averaged energy for the 3^-, 5^-, 7^-, and 9^- states by the dotted lines. These three bands have large overlaps with the basis wave function shown in Fig. 3(c), in which the longest axis of the deformed ^{24}Mg cluster is perpendicular to the inter-cluster coordinate between the ^{24}Mg and α clusters. The ground band is dominated by the mean-field configuration shown in Fig. 3(b), but it also has a non-negligible overlap with the cluster configuration shown in Fig. 3(c). Therefore, the ground band was also assigned as a member of the ^{24}Mg + α (T) bands. Because the ^{24}Mg cluster is considerably deformed, we expect that the rotational excitation of ^{24}Mg is coupled to the angular momentum of the inter-cluster motion in the RWAs. Experimentally, the corresponding cluster bands are not clearly identified, except for the ground band. In Fig. 3 we show several candidates for the ^{24}Mg + α cluster states observed by the α transfer reaction on ^{24}Mg [93,97].

To calculate the RWAs of the 0^+_1, 0^+_6, 1^-_1, and $1^-_{8,9,10}$ states, the cluster wave functions in the reference state are prepared as follows. The α cluster is assumed to have a $(0s)^4$ configuration and

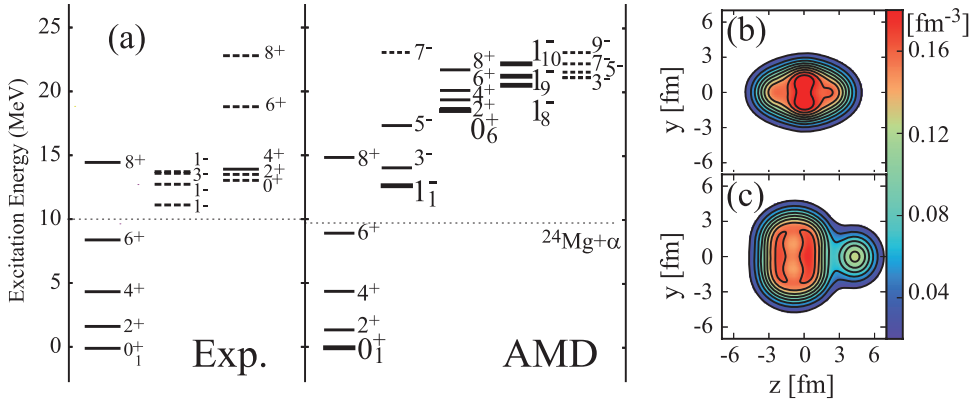

Fig. 3. (a) The calculated and observed partial level scheme of ^{28}Si corresponding to the ^{24}Mg + α cluster states. The dashed horizontal lines indicate experimental and theoretical ^{24}Mg + α threshold energies. (b) and (c) Intrinsic density distributions of the AMD wave functions which have the maximum overlap with the 0^+_1 and 0^+_6 states, respectively.

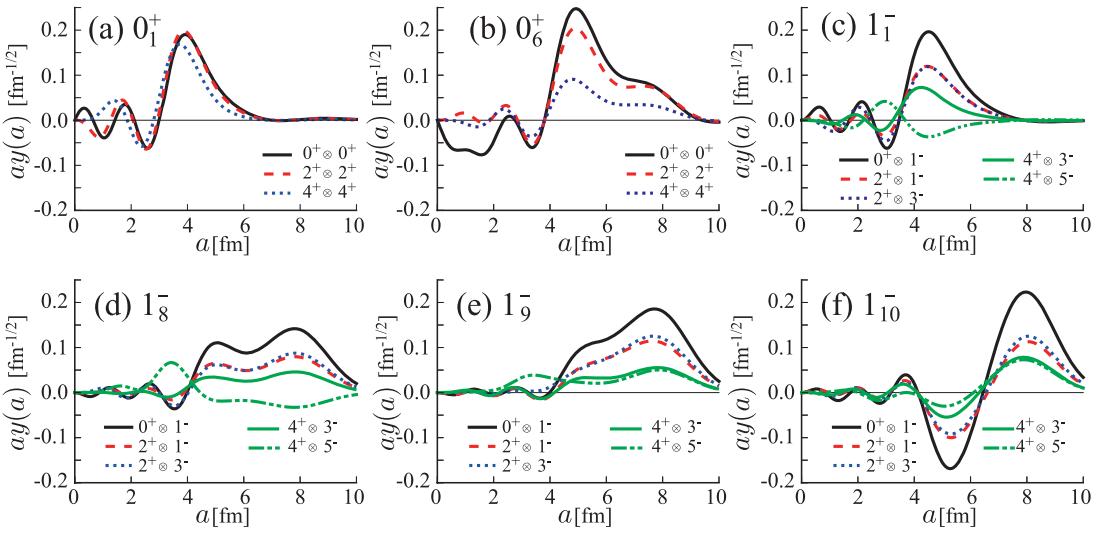

Fig. 4. The RWAs of the 0^+_1, 0^+_6, 1^-_8, 1^-_9, and 1^-_{10} states of ^{28}Si for ^{24}Mg+α cluster channels $j_2 \otimes l$ up to $j_2 = 4$ and $l = 5$.

Table 2. The calculated α spectroscopic factors S_α and the dimensionless decay widths θ^2_α of ^{24}Mg+α clustering in 0^+ states. The dimensionless decay widths are given in units of 10^{-2} and calculated with a channel radius of $a = 5$ and 9 fm for the 0^+_1 and 0^+_6 states, respectively.

	S_α			θ^2_α		
$j^\pi \otimes l^{(-)^l}$	$0^+\otimes 0^+$	$2^+\otimes 2^+$	$4^+\otimes 4^+$	$0^+\otimes 0^+$	$2^+\otimes 2^+$	$4^+\otimes 4^+$
0^+_1	0.05	0.05	0.03	1.1	1.0	0.3
0^+_6	0.11	0.07	0.01	1.1	1.0	0.2

its spherical oscillator parameter is set to $\nu_\alpha = 0.25\,\text{fm}^{-2}$. The AMD wave function for the ^{24}Mg cluster is calculated by energy variation, and it is projected to the 0^+, 2^+, and 4^+ states. The oscillator parameter is determined to minimize the energy of the 0^+ state. Because of the triaxial deformation of the ^{24}Mg, the optimum oscillator parameter is anisotropic and has different values for the x, y, and z directions: $\boldsymbol{\nu}_{\text{Mg}} = (0.12, 0.167, 0.169)\,\text{fm}^{-2}$. Using these cluster wave functions, the RWA is calculated for various combinations of the angular momenta. Denoting the parity and angular momentum of ^{24}Mg by j^π and those of the inter-cluster motion by $l^{(-)^l}$, the RWAs of the 0^+ states are calculated for the combinations $j^\pi \otimes l^{(-)^l} = 0^+ \otimes 0^+$, $2^+ \otimes 2^+$, and $4^+ \otimes 4^+$, and the RWAs of the 1^- states are calculated for $j^\pi \otimes l^{(-)^l} = 0^+ \otimes 1^-$, $2^+ \otimes 1^-$, $2^+ \otimes 3^-$, $4^+ \otimes 3^-$, and $4^+ \otimes 5^-$.

The results are presented in Fig. 4 and Tables 2 and 3. Although detailed discussions on RWAs and their relationship to the clustering in ^{28}Si will be made in our next work, we briefly comment here on the characteristics of the calculated RWAs.

The RWAs of the 0^+_1 and 1^- states show similar natures. These states are dominated by the mean-field configurations, and are under the strong influence of the spin–orbit interaction. Therefore, the clusters are considerably distorted and S_α is rather small. Nevertheless, we recognize a non-negligible cluster formation probability around the surface region of the nucleus ($a \simeq 4$ fm), which indicates the duality of the shell and cluster, as discussed in Ref. [84]. In terms of the $SU(3)$ shell model, the 0^+_1 and 1^-_1 states correspond to the $0\hbar\omega$ and $1\hbar\omega$ configurations, and hence the nodal quantum number n of RWAs should be equal to $n = (N - l)/2$, where N is 8 and 9 for the 0^+_1 and 1^- states, respectively.

Table 3. The calculated spectroscopic factors S_α and the dimensionless decay widths θ_α^2 of ^{24}Mg+α clustering in 1^- states. The dimensionless decay widths are given in units of 10^{-2} and calculated with a channel radius of $a = 6$ and 9 fm for the 1^-_1 and $1^-_{8,9,10}$ states, respectively.

S_α					
$j^\pi \otimes l^{(-)^l}$	$0^+ \otimes 1^-$	$2^+ \otimes 1^-$	$2^+ \otimes 3^-$	$4^+ \otimes 3^-$	$4^+ \otimes 5^-$
1^-_1	0.06	0.02	0.02	0.03	0.01
1^-_8	0.06	0.02	0.04	0.01	0.01
1^-_9	0.09	0.04	0.02	0.01	0.01
1^-_{10}	0.12	0.03	0.04	0.01	0.01
θ_α^2					
$j^\pi \otimes l^{(-)^l}$	$0^+ \otimes 1^-$	$2^+ \otimes 1^-$	$2^+ \otimes 3^-$	$4^+ \otimes 3^-$	$4^+ \otimes 5^-$
1^-_1	0.8	0.3	0.3	0.2×10^{-1}	0.5×10^{-1}
1^-_8	1.9	0.6	0.8	0.2	0.2
1^-_9	3.0	1.1	1.3	0.3	0.3
1^-_{10}	5.0	1.5	0.2	0.6	0.5

We clearly see that the calculated RWAs follow this relationship. For example, the $0^+ \otimes 0^+$ RWA has four nodes, while the $2^+ \otimes 2^+$ RWA has three.

Compared to the 0^+_1 and 1^-_1 states, the 0^+_6 and $1^-_{8,9,10}$ states have developed cluster structures. It is confirmed from their larger S_α and RWAs stretch outwards. Differently from the 0^+_1 and 1^-_1 states, their RWAs do not follow the relationship of $n = (N - l)/2$. This is due to mixing with other cluster and non-cluster configurations, which disturbs the behavior of RWAs. Indeed, we see that the RWAs, in particular those of the $1^-_{8,9,10}$ states, show irregular behavior in the inner and outer regions. This is consistent with the fact that the $^{24}\mathrm{Mg} + \alpha$ configuration is strongly mixed with non-cluster configurations and does not appear as a single state but appears as the $1^-_{8,9,10}$ states in this energy region. It is also noted that the RWAs in the $j^\pi \otimes l^{(-)^l} = 2^+ \otimes l^{(-)^l}$ and $4^+ \otimes l^{(-)^l}$ channels are as large as those of the $0^+ \otimes l^{(-)^l}$ channels, which reveals that the rotational excitation of ^{24}Mg is coupled to the inter-cluster motion, because of the large deformation of ^{24}Mg.

It must be emphasized that the RWAs shown in Fig. 4 are hardly ever obtained by the ordinary method because of the large computational cost required. Thus, the Laplace expansion method realizes accurate and detailed analysis of the clustering based on the RWAs, which is indispensable in discussing the clustering in heavier-mass and unstable nuclei.

4. Summary

In summary, we have presented a new method for RWA calculation named the Laplace expansion method. This method is based on the Laplace expansion and the analytical separation of the center-of-mass wave function, and is applicable to the Brink–Bloch and AMD wave functions. The method enables the calculation of RWA for unequal-sized and deformed clusters without any approximations. Furthermore, it allows the use of the GCM wave function for the cluster wave functions, which enables the calculation of the RWA of non-conventional clusters such as ^{6}He. Despite these advantages, the method does not require large computational cost, except for heavy-mass clusters.

Using the Laplace expansion method, we calculated the RWAs of the $^{16}\mathrm{O} + \alpha$ clustering as an example of unequal-sized clusters. It was found that the $^{16}\mathrm{O} + \alpha$ RWA calculated by using unequal-sized clusters tends to be smaller than the common-size case, and the difference amounts

to 10%–20%. We also presented the RWAs of the ^{24}Mg + α clustering as an example of deformed clusters. It was shown that the RWAs are considerably distorted, because of mixing with the cluster and non-cluster configurations. The RWAs also showed that the rotational excitation of ^{24}Mg is coupled to the inter-cluster motion, because of the large deformation of ^{24}Mg. Thus, the Laplace expansion method enables the calculation of RWA for various cluster systems, and we expect that it will be very helpful for the study of clustering in heavier-mass and unstable nuclei.

Acknowledgements

The authors thank Dr. Taniguchi for fruitful discussions. Support by Grants-in-Aid for Scientific Research on Innovative Areas from MEXT (Grant No. 2404:24105008) and JSPS KAKENHI Grant Nos. 16J03654 and 16K05339 is acknowledged.

Appendix A. Calculation of the overlaps needed in the Laplace expansion method

Here, we explain the calculation of the overlaps defined by Eqs. (34), (35), and (36). For an arbitrary matrix Γ, Eq. (34) is calculated by numerical integration:

$$\chi_{lm_l}(a; i_1, \ldots, i_A) = \left(\frac{|2\Gamma|}{\pi^3}\right)^{1/4} \int d\hat{a} Y^*_{lm_l}(\hat{a}) \exp\left\{-(\boldsymbol{a}-\boldsymbol{z})^{\mathrm{T}}\Gamma(\boldsymbol{a}-\boldsymbol{z})\right\}. \tag{A.1}$$

However, when $\chi(\boldsymbol{r}; i_1, \ldots, i_A)$ is a spherical Gaussian, i.e., when the matrix Γ is proportional to the identity matrix I as $\Gamma = \gamma I$, Eq. (A.1) has a simple analytical form:

$$\chi_{lm_l}(a; i_1, \ldots, i_A) = 4\pi i_l(2\gamma az) e^{-\gamma(a^2+z^2)} \frac{z^l Y^*_{lm_l}(\hat{z})}{z^l}, \tag{A.2}$$

where $i_l(2\gamma az)$ denotes the regular modified spherical Bessel function. The complex variable z is defined as $z = \sqrt{\boldsymbol{z}\cdot\boldsymbol{z}}$, and $z^l Y^*_{lm_l}(\hat{z})$ should be calculated in its Cartesian representation.

The overlap $N^{j_1\pi_1}_{m_1}(i_1, \ldots, i_{C_1})$ defined by Eq. (35) is calculated as follows. For simplicity, we first assume that the wave function $\Phi^{j_1\pi_1}_{m_1C_1}$ in the reference state is also represented by a single projected AMD wave function,

$$\Phi^{\mathrm{AMD}}_{C_1} = \Phi^{\mathrm{cm}}_{C_1}\Phi^{\mathrm{int}}_{C_1} = \frac{1}{\sqrt{C_1!}} \begin{vmatrix} \langle \boldsymbol{r}_1|\phi_{i_1}\rangle & \cdots & \langle \boldsymbol{r}_1|\phi_{i_{C_1}}\rangle \\ \vdots & \ddots & \vdots \\ \langle \boldsymbol{r}_{C_1}|\phi_{i_1}\rangle & \cdots & \langle \boldsymbol{r}_{C_1}|\phi_{i_{C_1}}\rangle \end{vmatrix}, \tag{A.3}$$

$$\Phi^{\mathrm{cm}}_{C_1} = \left(\frac{|2C_1 m|}{\pi^3}\right)^{1/4} \exp\left\{-C_1 \boldsymbol{R}^{\mathrm{T}}_{C_1} m \boldsymbol{R}_{C_1}\right\}, \tag{A.4}$$

$$\Phi^{j_1\pi_1}_{m_1C_1} = \frac{1}{\sqrt{n^{j_1\pi_1}_{k_1}}} \hat{P}^{j_1}_{m_1k_1}\hat{P}^{\pi_1}\Phi^{\mathrm{int}}_{C_1}, \quad n^{j_1\pi_1}_{k_1} = \langle \Phi^{\mathrm{int}}_{C_1}|\hat{P}^{j_1\pi_1}_{k_1k_1}|\Phi^{\mathrm{int}}_{C_1}\rangle\,. \tag{A.5}$$

Then, the overlap is given as

$$N^{j_1\pi_1}_{m_1}(i_1, \ldots, i_{C_1}) = \frac{2j_1+1}{8\pi^2\sqrt{n^{j_1\pi_1}_{k_1}}} \int d\Omega D^{j_1*}_{k_1m_1}(\Omega)\, \langle \Phi^{\mathrm{int}}_{C_1}|\hat{P}^{\pi_1}\hat{R}(\Omega)|\Psi^{\mathrm{int}}_{C_1}(i_1, \ldots, i_{C_1})\rangle\,, \tag{A.6}$$

where the integration over Euler angles is numerically calculated. To calculate the integrand in Eq. (A.6), we introduce an AMD wave function $\widetilde{\Psi}^{\rm AMD}_{C_1}$,

$$\widetilde{\Psi}^{\rm AMD}_{C_1}(i_1,\ldots,i_{C_1}) = \widetilde{\Psi}^{\rm cm}_{C_1}\Psi^{\rm int}_{C_1}(i_1,\ldots,i_{C_1}) = \frac{1}{\sqrt{C_1!}}\begin{vmatrix} \langle \boldsymbol{r}_1|\widetilde{\psi}_{i_1}\rangle & \cdots & \langle \boldsymbol{r}_1|\widetilde{\psi}_{i_{C_1}}\rangle \\ \vdots & \ddots & \vdots \\ \langle \boldsymbol{r}_{C_1}|\widetilde{\psi}_{i_1}\rangle & \cdots & \langle \boldsymbol{r}_{C_1}|\widetilde{\psi}_{i_{C_1}}\rangle \end{vmatrix}, \tag{A.7}$$

$$\langle \boldsymbol{r}|\widetilde{\psi}_i\rangle = \left(\frac{|2M|}{\pi^3}\right)^{1/4} \exp\left\{-(\boldsymbol{r}-\boldsymbol{Z}'_i)^{\rm T}M(\boldsymbol{r}-\boldsymbol{Z}'_i)\right\}(\alpha_i\chi_\uparrow + \beta_i\chi_\downarrow)\eta_i, \tag{A.8}$$

$$\widetilde{\Psi}^{\rm cm}_{C_1} = \left(\frac{|2C_1M|}{\pi^3}\right)^{1/4} \exp\left\{-C_1\boldsymbol{R}^{\rm T}_{C_1}M\boldsymbol{R}_{C_1}\right\}, \tag{A.9}$$

$$\boldsymbol{Z}'_i = \boldsymbol{Z}_i - \frac{1}{C_1}\sum_{j\in i_1,\ldots,i_{C_1}}\boldsymbol{Z}_j, \quad i\in\{i_1,\ldots,i_{C_1}\}, \tag{A.10}$$

where the Gaussian centroids are shifted from $\Psi^{\rm AMD}_{C_1}(i_1,...,i_{C_1})$ so that the center-of-mass wave function is located at the origin of the coordinate system. Note that this shift does not change the internal wave function. Therefore, the internal wave function of $\widetilde{\Psi}^{\rm AMD}_{C_1}$ is the same as the ket state of the integrand in Eq. (A.6). Using Eqs. (A.3) and (A.7), the overlap of AMD wave functions is calculated as

$$\langle\Phi^{\rm AMD}_{C_1}|\hat{P}^\pi\hat{R}(\Omega)|\widetilde{\Psi}^{\rm AMD}_{C_1}\rangle = \langle\Phi^{\rm int}_{C_1}|\hat{P}^\pi\hat{R}(\Omega)|\Psi^{\rm int}_{C_1}\rangle\,\langle\Phi^{\rm cm}_{C_1}|\hat{P}^\pi\hat{R}(\Omega)|\widetilde{\Psi}^{\rm cm}_{C_1}\rangle\,. \tag{A.11}$$

Here, the calculation of the left-hand side of Eq. (A.11) is straightforward, and the overlap of the center-of-mass wave functions is analytically calculated as

$$\langle\Phi^{\rm cm}_{C_1}|\hat{P}^\pi\hat{R}(\Omega)|\widetilde{\Psi}^{\rm cm}_{C_1}\rangle = \left(\frac{|2m||2M|}{|M'+m|^2}\right)^{1/4}, \tag{A.12}$$

$$M' = R^{\rm T}(\Omega)MR(\Omega), \tag{A.13}$$

where $R(\Omega)$ is a 3×3 rotation matrix which satisfies $\hat{R}(\Omega)\boldsymbol{R} = R(\Omega)\boldsymbol{R}$. Therefore, the integrand is proportional to the overlap of AMD wave functions:

$$\langle\Phi^{\rm int}_{C_1}|\hat{P}^\pi\hat{R}(\Omega)|\Psi^{\rm int}_{C_1}\rangle = \left(\frac{|M'+m|^2}{|2m||2M|}\right)^{1/4}\langle\Phi^{\rm AMD}_{C_1}|\hat{P}^\pi\hat{R}(\Omega)|\widetilde{\Psi}^{\rm AMD}_{C_1}\rangle\,. \tag{A.14}$$

It is clear that when $\Phi^{j_1\pi_1}_{C_1}$ and/or $\Psi^{j_1\pi_1}_{C_1}$ are not a single AMD wave function but a GCM wave function, the integrand is a superposition of Eq. (A.14).

Appendix B. An ordinary method for RWA calculation

To keep this paper self-contained, we explain an ordinary method for RWA calculation [70–73] that is often used in cluster models and AMD, and derive Eqs. (43), (44), (45), and (46). We start from the set of Brink–Bloch-type wave functions given in Eq. (40):

$$\Phi^{\rm BB}_{j_1\pi_1m_1j_2\pi_2m_2}(S_p) = n_0\mathcal{A}\left\{\hat{P}^{j_1}_{m_1k_1}\hat{P}^{\pi_1}\Phi_{C_1}\left(-\frac{C_2}{A}\boldsymbol{S}_p\right)\hat{P}^{j_2}_{m_2k_2}\hat{P}^{\pi_2}\Phi_{C_2}\left(\frac{C_1}{A}\boldsymbol{S}_p\right)\right\}, \tag{B.1}$$

$$n_0 = \sqrt{\frac{C_1!C_2!}{A!}}, \quad \boldsymbol{S}_p = (0,0,S_p), \tag{B.2}$$

where $\Phi_{C_1}\left(-C_2/A\boldsymbol{S}_p\right)$ and $\Phi_{C_2}\left(C_1/A\boldsymbol{S}_p\right)$ are the wave functions for clusters with masses C_1 and C_2, placed with an inter-cluster distance S_p. They are respectively projected to j^{π_1} and j^{π_2}. By assuming that Φ_{C_1} and Φ_{C_2} are the $SU(3)$ shell model wave functions without any particle–hole excitations and have the common oscillator parameter $\hbar\omega = 2\hbar^2\nu/m$, their internal and center-of-mass wave functions can be analytically separated:

$$\Phi_{C_1}\left(-\frac{C_2}{A}\boldsymbol{S}_p\right) = \Phi^{\rm int}_{C_1}\Phi^{\rm cm}_{C_1}, \quad \Phi^{\rm cm}_{C_1} = \left(\frac{2C_1\nu}{\pi}\right)^{3/4}\exp\left\{-C_1\nu(\boldsymbol{R}_{C_1} + \frac{C_2}{A}\boldsymbol{S}_p)^2\right\}, \tag{B.3}$$

$$\Phi_{C_2}\left(\frac{C_1}{A}\boldsymbol{S}_p\right) = \Phi^{\rm int}_{C_2}\Phi^{\rm cm}_{C_2}, \quad \Phi^{\rm cm}_{C_2} = \left(\frac{2C_2\nu}{\pi}\right)^{3/4}\exp\left\{-C_2\nu(\boldsymbol{R}_{C_2} - \frac{C_1}{A}\boldsymbol{S}_p)^2\right\}, \tag{B.4}$$

where $\boldsymbol{R}_{C_1}$ and $\boldsymbol{R}_{C_2}$ are the center-of-mass coordinates of the clusters defined by Eq. (22). In a similar way to Eq. (24), we rewrite the product of the center-of-mass wave functions as follows:

$$\Phi^{\rm cm}_{C_1}\Phi^{\rm cm}_{C_2} = \Phi^{\rm cm}_A\chi(\boldsymbol{r}), \tag{B.5}$$

$$\Phi^{\rm cm}_A = \left(\frac{2A\nu}{\pi}\right)^{3/4}\exp\left\{-A\nu R^2\right\}, \tag{B.6}$$

$$\chi(\boldsymbol{r}) = \left(\frac{2\gamma}{\pi}\right)^{3/4}\exp\left\{-\gamma(\boldsymbol{r}-\boldsymbol{S}_p)^2\right\}, \quad \gamma = \frac{C_1C_2}{A}\nu. \tag{B.7}$$

Here, $\boldsymbol{R}$ and $\boldsymbol{r}$ are the center-of-mass coordinate of the A-body system and the inter-cluster coordinate defined by Eqs. (5) and (26), respectively. Note that the oscillator parameters of the clusters should be the same, otherwise the decomposition to the center-of-mass and relative coordinates is not straightforward. Since the relative wave function Eq. (B.7) is the coherent state of HO except for a phase factor, it is represented by a superposition of the HO wave functions [71],

$$\chi(\boldsymbol{r}) = \sum_{Nl} a_{Nl}(S_p)R_{Nl}(r)Y_{l0}(\hat{r}), \tag{B.8}$$

$$a_{Nl}(S_p) = (-)^{(N-l)/2}\sqrt{\frac{(2l+1)N!}{(N-l)!!(N+l+1)!!}}\frac{(\gamma S_p^2)^{N/2}}{\sqrt{N!}}e^{-\gamma S_p^2/2}, \tag{B.9}$$

where $R_{Nl}(r)$ is the radial wave function of HO and N denotes the principal quantum number. With these equations, the Brink–Bloch-type wave function is rewritten as follows:

$$\Phi^{\rm BB}_{j_1\pi_1 m_1 j_2\pi_2 m_2}(S_p) = \Phi^{\rm cm}_A\sum_{Nl} a_{Nl}(S_p)n_0\mathcal{A}\left\{R_{Nl}(r)Y_{l0}(\hat{r})\Phi^{j_1}_{C_1m_1}\Phi^{j_2}_{C_2m_2}\right\}. \tag{B.10}$$

Then, by using the property of the angular momentum projector $P^J_{MK}\,|JK\rangle = |JM\rangle$ and the coupling of angular momenta, we introduce the wave function

$$\begin{aligned}\Phi^{J\pi}_{j_1\pi_1 j_2\pi_2 j_{12} l}(S_p) &= \frac{2l+1}{2J+1}\sum_{m_{12}m_1m_2} C^{Jm_{12}}_{l0m_{12}}\hat{P}^J_{Mm_{12}}C^{j_{12}m_{12}}_{j_1m_1j_2m_2}\Phi^{\rm BB}_{j_1\pi_1m_1j_2\pi_2m_2}(S_p)\\ &= \sum_N a_{Nl}(S_p)n_0\mathcal{A}\left\{R_{Nl}(r)\left[Y_l(\hat{r})\left[\Phi^{j_1\pi_1}_{C_1}\Phi^{j_2\pi_2}_{C_2}\right]_{j_{12}}\right]_{JM}\right\},\end{aligned} \tag{B.11}$$

in which the angular momenta of the clusters are coupled to j_{12}, and j_{12} is coupled with the orbital angular momentum of the relative motion l yielding the total angular momentum J. $\Phi^{j_1\pi_1}_{C_1}$ and $\Phi^{j_2\pi_2}_{C_2}$

denote the projected internal wave functions, $\Phi^{j_1\pi_1}_{C_1} = \hat{P}^{j_1}_{m_1k_1}\Phi^{\rm int}_{C_1}$ and $\Phi^{j_2\pi_2}_{C_2} = \hat{P}^{j_2}_{m_2k_2}\Phi^{\rm int}_{C_2}$. When the inter-cluster distance S_p, $p = 1,\ldots,p_{\rm max}$, is dense discretized, and the maximum (minimum) distance is chosen to be large (small) enough, a set of wave functions given by Eq. (B.11) should span the complete set for the $C_1 + C_2$ cluster states with the above-mentioned angular momentum coupling, i.e.,

$$\sum_{pq} |\Phi^{J\pi}_{j_1\pi_1 j_2\pi_2 j_{12} l}(S_p)\rangle\, B^{-1}_{pq}\, \langle\Phi^{J\pi}_{j_1\pi_1 j_2\pi_2 j_{12} l}(S_q)| \simeq 1, \tag{B.12}$$

$$B_{pq} = \langle\Phi^{J\pi}_{j_1\pi_1 j_2\pi_2 j_{12} l}(S_p)|\Phi^{J\pi}_{j_1\pi_1 j_2\pi_2 j_{12} l}(S_q)\rangle\,. \tag{B.13}$$

Inserting Eq. (B.12) into the definition of the RWA, we get

$$\begin{aligned} y^{J\pi}_{j_1\pi_1 j_2\pi_2 j_{12} l}(a) = &\sqrt{\frac{A!}{(1+\delta_{C_1C_2})C_1!C_2!}} \\ &\times \sum_{pq}\left\langle \frac{\delta(r-a)}{r^2}\left[Y_l(\hat{r})\left[\Phi^{j_1\pi_1}_{C_1}\Phi^{j_2\pi_2}_{C_2}\right]_{j_{12}}\right]_{JM}\middle|\,\Phi^{J\pi}_{j_1\pi_1 j_2\pi_2 j_{12} l}(S_p)\right\rangle \\ &\times B^{-1}_{pq}\,\langle\Phi^{J\pi}_{j_1\pi_1 j_2\pi_2 j_{12} l}(S_q)|\Psi^{J\pi}_{MA}\rangle\,. \end{aligned} \tag{B.14}$$

Using the completeness of the HO wave function $\sum_N R_{Nl}(r)R_{Nl}(a) = \delta(r-a)/r^2$ and Eq. (B.11), the braket in the second line reads

$$\begin{aligned} &\left\langle \frac{\delta(r-a)}{r^2}\left[Y_l(\hat{r})\left[\Phi^{j_1\pi_1}_{C_1}\Phi^{j_2\pi_2}_{C_2}\right]_{j_{12}}\right]_{JM}\middle|\,\Phi^{J\pi}_{j_1\pi_1 j_2\pi_2 j_{12} l}(S_p)\right\rangle = n_0\sum_{NN'} a_{N'l}(S_p)R_{Nl}(a) \\ &\quad\times\left\langle R_{Nl}(r)\left[Y_l(\hat{r})\left[\Phi^{j_1\pi_1}_{C_1}\Phi^{j_2\pi_2}_{C_2}\right]_{j_{12}}\right]_{JM}\middle|\,\mathcal{A}\left\{R_{N'l}(r)\left[Y_l(\hat{r})\left[\Phi^{j_1\pi_1}_{C_1}\Phi^{j_2\pi_2}_{C_2}\right]_{j_{12}}\right]_{JM}\right\}\right\rangle \\ &= n_0\sum_N a_{Nl}(S_p)\mu_{Nl}R_{Nl}(a). \end{aligned} \tag{B.15}$$

In the last line, we assumed that $\Phi^{j_1}_{C_1}$ and $\Phi^{j_2}_{C_2}$ are eigenstates of the principal quantum number $\hat{N}$. In this case, the braket in the second line is non-zero only when $N = N'$, and we denote it $\mu_N\delta_{NN'}$. From Eqs. (B.14) and (B.15), we get

$$y^{J\pi}_{j_1\pi_1 j_2\pi_2 j_{12} l}(a) = \frac{1}{\sqrt{1+\delta_{C_1C_2}}}\sum_N \mu_{Nl}\left(\sum_{pq} a_{Nl}(S_p)B^{-1}_{pq}\,\langle\Phi^{J\pi}_{j_1\pi_1 j_2\pi_2 j_{12} l}(S_q)|\Psi^{J\pi}_{MA}\rangle\right)R_{Nl}(a). \tag{B.16}$$

Simplifying this equation, we obtain Eqs. (43), (44), (45), and (46).

References

[1] K. Ikeda, N. Takigawa, and H. Horiuchi, Prog. Theor. Phys. Suppl. E **68**, 464 (1968).
[2] M. Seya, M. Kohno, and S. Nagata, Prog. Theor. Phys. **65**, 204 (1981).
[3] W. von Oertzen, Z. Phys. A Hadron. Nucl. **354**, 37 (1996).
[4] Y. Kanada-En'yo, H. Horiuchi, and A. Doté, Phys. Rev. C **60**, 064304 (1999).
[5] N. Itagaki and S. Okabe, Phys. Rev. C **61**, 044306 (2000).
[6] P. Descouvemont, Nucl. Phys. A **699**, 463 (2002).
[7] M. Freer et al., Phys. Rev. Lett. **82**, 1383 (1999).
[8] M. Freer et al., Phys. Rev. C **63**, 034301 (2001).
[9] N. Curtis et al., Phys. Rev. C **70**, 014305 (2004).

[10] M. Milin et al., Nucl. Phys. A **753**, 263 (2005).
[11] H. G. Bohlen, T. Dorsch, Tz. Kokalova, W. von Oertzen, Ch. Schulz, and C. Wheldon, Phys. Rev. C **75**, 054604 (2007).
[12] P Descouvemont and D Baye, Rep. Prog. Phys. **73**, 036301 (2010).
[13] F. Nemoto and H. Bandō, Prog. Theor. Phys. **47**, 1210 (1972).
[14] W. Sünkel and K. Wildermuth, Phys. Lett. B **41**, 439 (1972).
[15] T. Matsuse and M. Kamimura, Prog. Theor. Phys. **49**, 1765 (1973).
[16] Y. Fujiwara et al., Prog. Theor. Phys. Suppl. **68**, 29 (1980).
[17] P. Descouvemont and D. Baye, Phys. Rev. C **36**, 54 (1987).
[18] U. Strohbusch, C. L. Fink, B. Zeidman, R. G. Markham, H. W. Fulbright, and R. N. Horoshko, Phys. Rev. C **9**, 965 (1974).
[19] H. Friedrich and K. Langanke, Nucl. Phys. A **252**, 47 (1975).
[20] R. R. Betts, H. T. Fortune, J. N. Bishop, M. N. I. Al-Jadir, and R. Middleton, Nucl. Phys. A **292**, 281 (1977).
[21] H. T. Fortune, M. N. I. Al-Jadir, R. R. Betts, J. N. Bishop, and R. Middleton, Phys. Rev. C **19**, 756 (1979).
[22] S. Ohkubo and K. Umehara, Prog. Theor. Phys. **80**, 598 (1988).
[23] T. Wada and H. Horiuchi, Phys. Rev. C **38**, 2063 (1988).
[24] T. Yamaya, S. Ohkubo, S. Okabe, and M. Fujiwara, Phys. Rev. C **47**, 2389 (1993).
[25] T. Yamaya, M. Saitoh, M. Fujiwara, T. Itahashi, K. Katori, T. Suehiro, S. Kato, S. Hatori, and S. Ohkubo, Nucl. Phys. A **573**, 154 (1994).
[26] F. Michel, S. Ohkubo, and G. Reidemeister, Prog. Theor. Phys. Suppl. **132**, 7 (1998).
[27] T. Yamaya, K. Katori, M. Fujiwara, S. Kato, and S. Ohkubo, Prog. Theor. Phys. Suppl. **132**, 73 (1998).
[28] M. Kimura and H. Horiuchi, Nucl. Phys. A **767**, 58 (2006).
[29] A. Tohsaki, H. Horiuchi, P. Schuck, and G. Röpke, Phys. Rev. Lett. **87**, 192501 (2001).
[30] T. Kawabata et al., Phys. Lett. B **646**, 6 (2007).
[31] Y. Kanada-En'yo, Phys. Rev. C **75**, 024302 (2007).
[32] T. Wakasa et al., Phys. Lett. B **653**, 173 (2007).
[33] T. Kawabata et al., Int. J. Mod. Phys. E **17**, 2071 (2008).
[34] Y. Funaki, T. Yamada, H. Horiuchi, G. Röpke, P. Schuck, and A. Tohsaki, Phys. Rev. Lett. **101**, 082502 (2008).
[35] M. Itoh et al., Phys. Rev. C **84**, 054308 (2011).
[36] T. Yamada, Y. Funaki, H. Horiuchi, K. Ikeda, and A. Tohsaki, Prog. Theor. Phys. **120**, 1139 (2008).
[37] T. Kawabata et al., J. Phys. Conf. Ser. **436**, 012009 (2013).
[38] M. Itoh et al., Phys. Rev. C **88**, 064313 (2013).
[39] Y. Chiba and M. Kimura, Phys. Rev. C **91**, 061302 (2015).
[40] Y. Kanada-En'yo, Phys. Rev. C **93**, 054307 (2016).
[41] Y. Chiba, M. Kimura, and Y. Taniguchi, Phys. Rev. C **93**, 034319 (2016).
[42] W. Scholz, P. Neogy, K. Bethge, and R. Middleton, Phys. Rev. C **6**, 893 (1972).
[43] P. Descouvemont and D. Baye, Phys. Rev. C **31**, 2274 (1985).
[44] P. Descouvemont, Phys. Rev. C **38**, 2397 (1988).
[45] G. V. Rogachev et al., Phys. Rev. C **64**, 051302 (2001).
[46] N. Curtis, D. D. Caussyn, C. Chandler, M. W. Cooper, N. R. Fletcher, R. W. Laird, and J. Pavan, Phys. Rev. C **66**, 024315 (2002).
[47] V. Z. Goldberg et al., Phys. Rev. C **69**, 024602 (2004).
[48] S. Yildiz et al., Phys. Rev. C **73**, 034601 (2006).
[49] M. Kimura, Phys. Rev. C **75**, 034312 (2007).
[50] N. Furutachi, M. Kimura, A. Dote, Y. Kanada-En'yo, and S. Oryu, Prog. Theor. Phys. **119**, 403 (2008).
[51] C. Fu et al., Phys. Rev. C **77**, 064314 (2008).
[52] E. D. Johnson et al., Eur. Phys. J. A **42**, 135 (2009).
[53] W. von Oertzen et al., Eur. Phys. J. A **43**, 17 (2010).
[54] N. Soić et al., Phys. Rev. C **68**, 014321 (2003).
[55] W. von Oertzen et al., Eur. Phys. J. A **21**, 193 (2004).
[56] D. L. Price et al., Phys. Rev. C **75**, 014305 (2007).
[57] P. J. Haigh et al., Phys. Rev. C **78**, 014319 (2008).

[58] T. Suhara and Y. Kanada-En'yo, Phys. Rev. C **82**, 044301 (2010).
[59] M. Freer et al., Phys. Rev. C **90**, 054324 (2014).
[60] T. Baba, Y. Chiba, and M. Kimura, Phys. Rev. C **90**, 064319 (2014).
[61] Z. Y. Tian et al., Chin. Phys. C **40**, 111001 (2016).
[62] D. Dell'Aquila et al., Phys. Rev. C **93**, 024611 (2016).
[63] A. Fritsch et al., Phys. Rev. C **93**, 014321 (2016).
[64] T. Baba and M. Kimura, Phys. Rev. C **94**, 044303 (2016).
[65] H. Yamaguchi et al., Phys. Lett. B **766**, 11 (2017).
[66] J. Li et al., Phys. Rev. C **95**, 021303 (2017).
[67] T. Baba and M. Kimura, arXiv:1702.04874 [nucl-th] [Search INSPIRE].
[68] V. V. Balashov, V. G. Neudachin, Yu. F. Smirnov, and N. P. Yudin, J. Exp. Theor. Phys. **37**, 1385 (1959).
[69] T. Honda, H. Horie, Y. Kudo, and H. UI, Nucl. Phys. **62**, 561 (1965).
[70] H. Horiuchi, Prog. Theor. Phys. **47**, 1058 (1972).
[71] H. Horiuchi, Prog. Theor. Phys. Suppl. **62**, 90 (1977).
[72] Y. Kanada-En'yo and H. Horiuchi, Phys. Rev. C **68**, 014319 (2003).
[73] M. Kimura, Phys. Rev. C **69**, 044319 (2004).
[74] J. P. Elliott, Proc. R. Soc. London A Math. Phys. Eng. Sci. **245**, 1240 (1958).
[75] J. P. Elliott, Proc. R. Soc. London A Math. Phys. Eng. Sci. **245**, 1243 (1958).
[76] Y. Kanada-En'yo, T. Suhara, and Y. Taniguchi, Prog. Theor. Exp. Phys. **2014**, 073D02 (2014).
[77] Y. Kanada-En'yo, M. Kimura, and H. Horiuchi, Comptes Rendus Phys. **4**, 497 (2003).
[78] Y. Kanada-En'yo, M. Kimura, and A. Ono, Prog. Theor. Exp. Phys. **2012**, 01A202 (2012).
[79] M. Kimura, T. Suhara, and Y. Kanada-En'yo, Eur. Phys. J. A **52**, 373 (2016).
[80] D. M. Brink, *Proc. Int. School of Physics Enrico Fermi, Course 36, Varenna* (Academic Press, New York, 1966).
[81] A. Tohsaki-Suzuki, Prog. Theor. Phys. **59**, 1261 (1978).
[82] M. Kimura and H. Horiuchi, Phys. Rev. C **69**, 051304 (2004).
[83] Y. Taniguchi, Y. Kanada-En'yo, and M. Kimura, Phys. Rev. C **80**, 044316 (2009).
[84] Y. Chiba, Y. Taniguchi, and M. Kimura, arXiv:1610.04000 [nucl-th] [Search INSPIRE].
[85] J. F. Berger, M. Girod, and D. Gogny, Comput. Phys. Commun. **63**, 365 (1991).
[86] H. Horiuchi, K. Ikeda, and Y. Suzuki, Prog. Theor. Phys. Suppl. **52**, 89 (1972).
[87] N. K. Glendenning, Phys. Rev. B **137**, 102 (1965).
[88] M. Kawai and K. Yazaki, Prog. Theor. Phys. **38**, 850 (1967).
[89] M. Igarashi, M. Kawai, and K. Yazaki, Prog. Theor. Phys. **42**, 245 (1969).
[90] R. Stokstad, D. Shapira, L. Chua, P. Parker, M. W. Sachs, R. Wieland, and D. A. Bromley, Phys. Rev. Lett. **28**, 1523 (1972).
[91] D. Baye, Nucl. Phys. A **272**, 445 (1976).
[92] J. W. Maas, E. Somorjai, H. D. Graber, C. A. Van Den Wijngaart, C. Van Der Leun, and P. M. Endt, Nucl. Phys. A **301**, 213 (1978).
[93] J. Cseh, E. Koltay, Z. Máté, E. Somorjai, and L. Zolnai, Nucl. Phys. A **385**, 43 (1982).
[94] T. Tanabe et al., Nucl. Phys. A **399**, 241 (1983).
[95] K. Kato, S. Okabe, and Y. Abe, Prog. Theor. Phys. **74**, 1053 (1985).
[96] S. Kubono, K. Morita, M. H. Tanaka, A. Sakaguchi, M. Sugitani, and S. Kato, Nucl. Phys. A **457**, 461 (1986).
[97] K. P. Artemov et al., Sov. J. Nucl. Phys. **51**, 777 (1990).
[98] N. I. Ashwood et al., Phys. Rev. C **63**, 034315 (2001).
[99] M. Shawcross et al., Phys. Rev. C **63**, 034311 (2001).
[100] A. Goasduff et al., Phys. Rev. C **89**, 014305 (2014).
[101] M. Kimura, R. Yoshida, and M. Isaka, Prog. Theor. Phys. **127**, 287 (2012).
[102] Y. Taniguchi, M. Kimura, and H. Horiuchi, Prog. Theor. Phys. **112**, 475 (2004).